Biometric Recognition via Eye Movements: Saccadic Vigor and Acceleration Cues

IOANNIS RIGAS AND OLEG KOMOGORTSEV, Texas State University
REZA SHADMEHR, John Hopkins University

Previous research shows that the human eye movements can serve as a valuable source of information about the structural elements of the oculomotor system, and also, they can open a window to the neural functions and the cognitive mechanisms related to visual attention and perception. The research field of eye movement-driven biometrics explores the extraction of individual-specific characteristics from the eye movements, and their employment for recognition purposes. In this work, we present a study for the incorporation of dynamic saccadic features into a model of eye movement-driven biometrics. We show that when these features are added to our previous biometric framework and tested on a large database of 322 subjects, the biometric accuracy presents a relative improvement in range of 31.6%-33.5% for the verification scenario, and in range of 22.3%-53.1% for the identification scenario. More importantly, this improvement is demonstrated for different types of visual stimulus (random dot, text, video), indicating the enhanced robustness offered by the incorporation of saccadic vigor and acceleration cues.

Categories and Subject Descriptors: **H.1.2 [Models and Principles]**: User/Machine Systems—*Human Information Processing*; **I.5.1 [Pattern Recognition]**: Models—*Statistical*

General Terms: Human Factors

Additional Key Words and Phrases: eye movement biometrics, saccadic vigor, saccadic acceleration

ACM Reference Format:

1. INTRODUCTION

Human eye movements serve as a vital mechanism for selection of information from the visual environment. The physical structure of the oculomotor system is formed by the eye globe, six extra-ocular muscles working in agonist-antagonist pairs, and various surrounding tissues, liquids, and ligaments. From the six extra-ocular muscles, the lateral and medial recti are responsible for horizontal eye movements, the superior and inferior recti are responsible for vertical eye movements, and the superior and inferior oblique are mainly responsible for torsional eye movements. The movements of the eye are coordinated by sequences of brain generated pulses transferred via the oculumotor nerve (for the medial, superior, inferior recti and inferior oblique muscles), the trochlear nerve (for the superior oblique muscle), and the abducens nerve (for the lateral rectus muscle) [Leigh and Zee 2006].

The first systematic studies of eye movements were conducted in the late 19th century, and involved the investigation of eye movements during reading [Javal 1878]. These early studies showed

This work is supported in part by the NSF CAREER Grant #CNS-1250718 and the NIST Grant #60NANB14D274. Special gratitude is expressed to Dr. Evgeny Abdulin, T. Miller, Ch. Heinich, and N. Myers for proctoring eye movement recordings.
Author's address: I. Rigas, Texas State University, Department of Computer Science, 601 University Drive, San Marcos, Texas 78666; email: rigas@txstate.edu; O. Komogortsev, Texas State University, Department of Computer Science, 601 University Drive, San Marcos, Texas 78666; email: ok11@txstate.edu; Reza Shadmehr, Johns Hopkins University, 720 Rutland Ave, 410 Traylor Building, Baltimore, MD 21205-2195; email: shadmehr@jhu.edu.

DOI:http://dx.doi.org/10.1145/0000000.0000000

that when a person processes a visual stimulus (e.g. text), the eyes do not move in a homogeneous (continuous) manner but make extremely fast movements from one point of focus to another. These fast movements are called *saccades*, and the points of focus are called *fixations*. In the following years, research regarding eye movements during different visual processing tasks progressed further [Buswell 1935; Just and Carpenter 1980; Yarbus 1967]. A specific branch of research investigated the relation between eye movements and perception. The experiments of [Eckstein et al. 2007] showed the existence of similarly activated neural mechanisms for perception and oculomotor action during visual search, whereas the work of [Collins and Doré-Mazars 2006] investigated the effects of saccadic adaptation in perception. Furthermore, there were various studies exploring the interconnections between eye movements and selective attention [Holcomb et al. 1977; Kowler et al. 1995]. A more detailed review of the research studies related to the eye movements and perception can be found in [Schutz et al. 2011]. The research of [Noton and Stark 1971a; Noton and Stark 1971b] and [Choi et al. 2014] showed that apart from the visual stimulus and the executed task, the eye movement strategies can also be influenced by idiosyncratic characteristics of the subject. The existence of intra-subject similarities in the performed eye movement patterns was also reported in the study of [Schnitzer and Kowler 2006], where the eye movement activity was explored in the case of repeated readings of text.

The findings of the above studies can support the research of eye movements as a source of biometric information. Generation of eye movements involves two mechanisms that can produce inter-subject differences: i) the physical oculomotor structure of every person, and ii) the brain activity supporting functions of vision which can be connected to cognition and perception [Choi et al. 2014]. The newly established research field of eye movement biometrics utilizes the inter-person dissimilarities in the execution of eye movements, and concentrates on the formation, comparison and classification of the respective biometric templates. Although the reliability of the eye movement biometrics is still not comparable to the traditional biometric recognition approaches like iris scanning, utilization of eye movement biometric cues can offer substantial advantages in terms of spoofing resistance [Komogortsev et al. 2015]. The functional components of the oculomotor system (eye globe, extraocular muscles, and brain stem) are well hidden inside of the eye cavity, and their manifestation in the form of eye movements is not static and cannot be replicated from a single image, as it can be potentially done for modalities like the fingerprints, face, and iris [Marcel et al. 2014]. Eye movements can be captured remotely and in an unobtrusive way along with other biometric modalities from the eye region, such as the iris [Komogortsev et al. 2012b]. Thus, they provide an appealing natural interface for the extraction of biometric information during the interaction with future wearable devices, e.g. Google Glass [Google]. Finally, because eye movements are a product of the human visual system that engages a variety of brain regions, manifestation of the pathologies occurring in those regions can be detected in the features extracted from eye movements. An example involves the use of eye movements for the detection of mild traumatic brain injuries [Cifu et al. 2015; Komogortsev and Holland 2014]. In particular, [Shadmehr et al. 2010] has suggested that the speed with which the eyes move during a saccade, i.e., saccade vigor, may be a reflection of between subject differences in patterns of decision-making in health and disease. Also, eye movements can be used for the evaluation of a user's fatigue [Abdulin and Komogortsev 2015; Yingying et al. 2014]. To this context, the extraction of biometric features from the eye movements provides a unique opportunity for the creation of 'smart biometric systems', which combine recognition and health monitoring using the same hardware and software.

1.1 Prior Art

The initial potential of eye movement biometrics was demonstrated in the work of [Kasprowski and Ober 2004]. The analysis of eye movement characteristics using the Cepstrum transform brought

about a False Acceptance Rate[1] (FAR) of 1.36% and a False Rejection Rate[1] (FRR) of 12.59% for a small test database of 9 persons. Subsequent studies were based on a similar rationale, and applied signal processing techniques already used in other domains. In the work of [Bednarik et al. 2005], properties of eye movement signals were inspected by applying the Fast Fourier Transform (FFT) and Principal Component Analysis (PCA). The best result for dynamic eye movement features and for a database of 12 persons was a classification rate (correct identification) of 56%. In the work of [Kinnunen et al. 2010], techniques from the field of voice recognition were applied on eye movement signals for achieving an Equal Error Rate[1] (EER) of 30% for a database of 17 persons.

The work presented in [Komogortsev et al. 2012a] proposed a methodology based on the use of a model of the oculomotor system for the simulation of eye saccades. By comparing the simulated eye movements with real ones, a set of modeling features was extracted and then used for biometric verification of human subjects. The achieved Half Total Error Rate (i.e. the average of FAR and FRR) for 59 subjects was 19%. The method was further modified in [Komogortsev et al. 2014b] and tested both on a high-resolution database (32 subjects) and on a low-resolution database (172 subjects). The achieved EER for the first database was 20.3% and the Rank-1 Identification Rate[1] (Rank-1 IR) was 65.7%, whereas for the second database the EER was 22.2% and the Rank-1 IR was 12.6%.

Another category of techniques examined the spatial distribution of eye movements with respect to the visual stimulus. A characteristic example of this category is the graph-based technique presented in [Rigas et al. 2012a]. In this case the multivariate Wald-Wolfowitz runs test was used for the comparison of the spatial distributions of fixation points. The achieved EER for a dataset of 15 subjects was 30%, and the identification rate was 70%. In the work of [Cantoni et al. 2015], a gaze analysis technique (GANT) based on graph modeling was tested for a larger population of 112 subjects, achieving a Rank-1 IR of 31.25% and an EER of 22.4%. An alternative spatial representation was proposed in [Rigas and Komogortsev 2014], with the use of a set of probabilistic activation maps (fixation density maps-FDM) for the representation of the fixation point distributions during the observation of video sequences. The achieved performances for single enrollments and for a large database recorded from 200 subjects were a top Rank-1 IR of 32.8% and a minimal EER of 12.1%.

A large number of methods investigated the extraction and employment of features describing the properties of fixation and saccadic profiles. In the work of [Rigas et al. 2012b], the graph-based scheme previously used in [Rigas et al. 2012a] was employed in order to compare velocity and acceleration features extracted from the fixation profiles. The method achieved Rank-1 IR of 82% for a database of 79 subjects and 91.5% for a smaller database of 37 subjects. In the work presented by [Holland and Komogortsev 2013a], different characteristics from fixations and saccades were modeled using a Gaussian CDF and combined using a weighted fusion scheme. Databases with different numbers of subjects were used (22, 32, 173 subjects), with the best EER being 28% and Rank-1 IR being 53% (for the database of 32 subjects). The method was improved to the Complex Eye Movement Behavior (CEM-B) framework presented in [Holland and Komogortsev 2013b], where the distributions of primitive characteristics of the fixations and saccades, related to duration, amplitude and velocity, were compared using different statistical tests (Ansari-Bradley, Mann-Whitney U-test, Kolmogorov-Smirnov, and Cramér-von Mises). The performance for a database of 32 subjects was a minimal EER of 16.5% and Rank-1 IR of 82.6%. In the work presented by [Zhang and Juhola 2012], data mining techniques (Neural Networks, SVM, RBF) were applied on saccadic features (amplitude, accuracy, latency, velocity and acceleration), reporting a verification rate of about 90% for a database of 132 subjects. Also, the study of [Yoon et al. 2014] used Hidden Markov Models (HMM) in order to model the relationships between gaze velocities in the case of cognitive visual stimulus composed of dot patterns. The classification performance for a small pool of 12 subjects ranged between 53%-76%.

[1] For definitions of performance metrics see Section 4.1

1.2 Motivation and Contribution

In this work, we present a comprehensive investigation of the effects from the integration of dynamic cues modeling the saccadic properties into the Complex Eye Movement Behavior (CEM-B) framework [Holland and Komogortsev 2013b]. The proposed scheme is based on the representation of the saccadic vigor as an expression of the peak velocity and amplitude relationship [Choi et al. 2014], and on the modeling of the saccadic acceleration and deceleration characteristics. The selected baseline biometric framework (CEM-B) in which the new features are integrated, has already shown its efficacy for more simple features such as the duration, amplitude, and velocity of eye movements. We hypothesize that the incorporation of features that model more complex phenomena encoded in the eye movements should improve the overall biometric performance. In order to test our hypothesis, we perform an extensive evaluation of the effects from the integration of the new dynamic features in terms of recognition accuracy and robustness when using different types of visual stimulus.

The motivation for exploring the biometric potential of saccadic vigor was inspired by the recent work of [Choi et al. 2014], investigating the relationship between the saccadic vigor and the impulsivity of subjects in the case of a decision-making task. The results in this study showed existence of a particular degree of idiosyncrasy in the saccadic vigor, which was correlated with the decision-making behavior, i.e. subjects with higher vigor had a steep temporal discount function during the decision-making task. Also, previous studies have associated the vigor of a saccadic movement with the activity of the 'buildup' cells in the intermediate layers of the superior colliculus (SC) [Ikeda and Hikosaka 2007], the primary integrating area for the eye movements.

Our work also explores the relationship between the acceleration and the deceleration of saccadic eye movements by modeling the characteristics of the saccadic acceleration profiles. In the past, the variability of dynamic saccadic features like the peak velocity and the magnitude of the peak acceleration were explored by [Abrams et al. 1989]. The acceleration of a moving body (e.g. the eye globe) reflects the properties of the mechanisms that apply the moving forces, in this case the muscles and the neural pulse signals. The work of [Carlton and Newell 1988] showed that the variability in the maximum acceleration can provide indications about the variability of the force parameters. Thus, we can hypothesize that the examination of the saccadic acceleration profile can provide information for the possible differences in the viscosity/elasticity of the muscles and/or their control functions.

The contribution of our work in the field of eye movement biometrics can be summarized as follows:

- We employ saccadic vigor as a biometric trait.
- We employ features modeling saccadic acceleration as a biometric trait.
- We evaluate the improvement afforded by saccadic vigor and acceleration over previous baseline.
- We investigate the robustness of the new biometric scheme for different visual stimuli.

2. METHODS

In this section, we describe the theoretical background related to the extraction of the saccadic vigor and acceleration features and their incorporation into the Complex Eye Movement Behavior (CEM-B) biometrics framework.

2.1 Modeling of Saccadic Vigor Features

The exploration of the relationships governing the basic characteristics of the saccades, e.g. the duration, the amplitude, and the peak velocity has been the topic of various studies in the past. The work presented by [Bahill et al. 1975], established the term 'main sequence' (borrowed from Astronomy) in order to describe the relationships between peak velocity and duration, and peak velocity and amplitude (or magnitude) of the saccadic eye movements. It was observed that the peak velocity increases almost linearly with saccadic duration, whereas the relationship between the peak

velocity and saccadic amplitude deviates from linearity for saccades of increasing amplitude, until it reaches a plateau. These findings were partially supported also by previous studies in the field [Robinson 1964; Zuber et al. 1965]. Despite the generally stereotyped behavior of the saccadic characteristics, their exact values can vary due to several reasons. The main sources of the variability in the characteristics modeled by the 'main sequence' have been researched by a number of studies in the past [Abrams, Meyer and Kornblum 1989; Bahill et al. 1981; Bollen et al. 1993]. Furthermore, the 'main sequence' and the variability of the saccadic characteristics have been explored in more recent studies using video-based eye-trackers [Di Stasi et al. 2011; Haith et al. 2012; van Beers 2007].

In Fig. 1 we demonstrate the 'main sequence' diagrams representing the saccades recorded from different subjects of our database. For comparison reasons, all the plots show the peak velocity-amplitude relationship for the horizontal component of the eye movement. In the specific experiment the subjects were observing a 'random jumping' dot of light, and thus, saccades of various amplitudes were acquired. A curve is fitted to the scattered data in order to exhibit the non-linear shape of the 'main sequence'. During the processing of the recordings any saccades with peak velocities > 1000°/s, and amplitudes > 100° were filtered out, since these values cannot physically represent actual saccades and they should be attributed to various recording artifacts, e.g. eye blinks. A first observation of the data verifies the theoretically expected behavior of the 'main sequence', which deviates from linearity as the saccadic amplitudes get larger. A closer inspection reveals noticeable inter-subject variations in the data-fitted shape of the 'main sequence', and also, in the exact degree of data scattering (dispersion from the fitted curve).

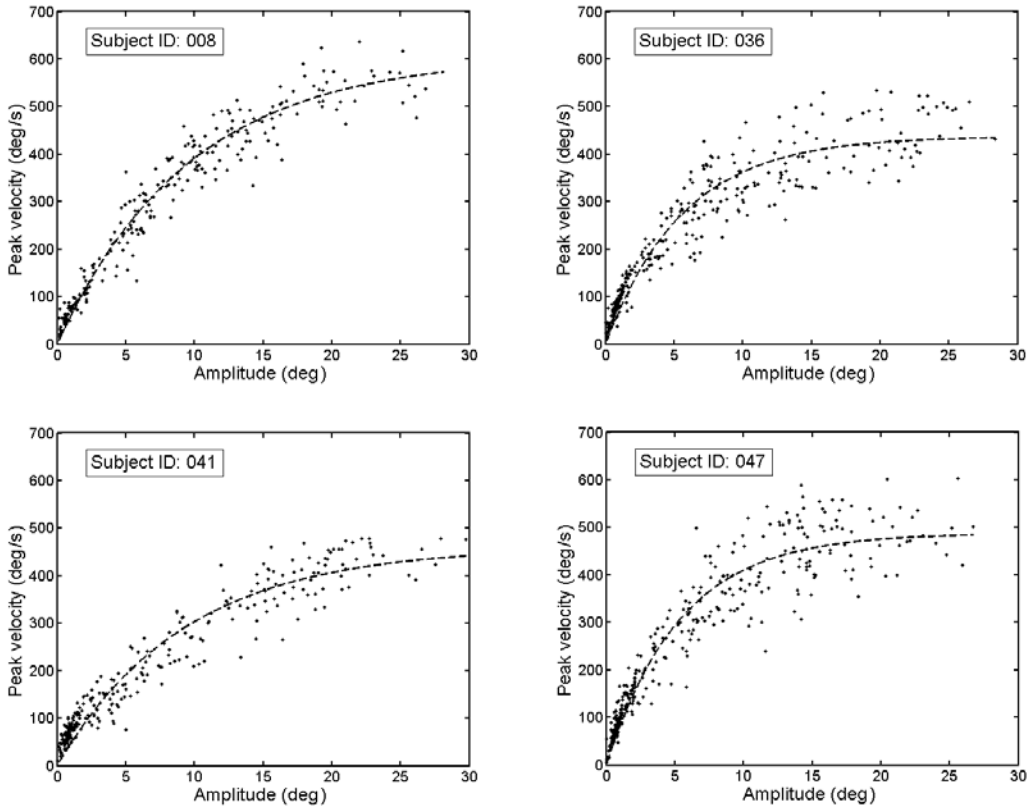

Fig. 1. Representation of the peak velocity-amplitude relationship ('main sequence') for saccades recorded from different subjects of our database. In all cases the figure shows the horizontal component of the eye movement.

The work presented recently by [Choi et al. 2014], investigated the saccadic vigor as an expression of the peak velocity-amplitude relationship in relation to the decision-making cost. The findings of this work supported that if we denote the across subject peak velocity-amplitude function with *g(x)*, then, we can approximate the peak velocity of saccade *j* for subject *i* as a scaled version of this function:

$$v_i^{(j)} = a_i \cdot g\left(x_i^{(j)}\right) \quad (1)$$

The scaling factor a_i can be employed as a gauge of the vigor of saccades for subject *i*. The conducted experiments showed that the values of vigor can present an idiosyncratic nature, and also, they appear to be closely related with the anticipation behavior of every subject *i*. Based on these findings, we explored the inter-subject variability of the saccadic vigor and investigated its potential as a biometric feature. To this purpose, we calculated the vigor of saccades performed by a subject during the observation of visual stimuli. The feature vectors were formed by the distributions of the extracted vigor values and were integrated into the biometric templates. The use of the vigor-value distributions instead of a unique value from the entire recording was opted as a more robust approach for capturing any subject-specific behavior differences during the manifestation of vigor over time.

The saccadic peak velocities can be determined by the respective saccadic velocity profiles. The procedure for the calculation of velocity involves the first order derivative of the eye movement positional signal. Computing a derivative can emphasize the presence of noise, especially for eye-trackers operating at high frequencies, as the one used in our experiments. Thus, for the calculation of velocity from the positional signal we opted to use the smoothing derivative formula proposed by [Bahill and McDonald 1983]. Let us denote the raw positional eye movement signal with *x*, and the sampling period with T_s. The formula for calculating the velocity of the *k-th* sample is the following:

$$v(k) = \left(x(k+3) - x(k-3)\right) \Big/ \left(6 \cdot T_s\right) \quad (2)$$

Assuming a sampling frequency of 1000 Hz, the achieved cut-off frequency (-3dB) is higher than 75 Hz, and the significant information about saccades is not filtered out [Bahill and McDonald 1983].

Using the calculated velocity signal, we can extract the velocity profiles for the individual saccades of a recording. First, we need to partition the eye movement recording into sequences of individual fixations and saccades. To this purpose, we employ the velocity threshold classification algorithm (I-VT) described in [Salvucci and Goldberg 2000]. The specific algorithm takes as an input the smoothed velocity signal calculated using Eq. (2), and after its parameterization it classifies all the samples with the velocity over a threshold as belonging to a saccade (otherwise they belong to a fixation). During the second step of the algorithm, the samples that are classified as belonging to a saccade (or fixation) are merged in order to form the profiles of the individual saccades (or fixations) performed by the subject. In our current incarnation of the algorithm we use a velocity threshold of 30°/s. Also, a 'micro-saccadic' filter is applied in order to reclassify any saccades with an amplitude < 0.5° (micro-saccades), and a 'micro-fixation' filter is applied in order to reclassify any fixations with a duration < 100 ms. The values employed for the velocity and the post-filtering thresholds are based on the normative values of human eye movement data [Leigh and Zee 2006]. As the I-VT algorithm does not restrict the detection only to saccades occurring directly after some specific changes in the visual stimulus, it can also detect spontaneous saccades. Also, the specific implementation of the I-VT algorithm cannot detect more complex movements like the smooth pursuits.

The first step for modeling the vigor of individual saccades is to determine a suitable generic non-linear function for representing the parametric relationship between the peak velocity and the amplitude of the saccades. Different empirical functions can be used for fitting the data, and in the current work we employ the following inverse exponential function proposed by [Baloh et al. 1975]:

$$y = a\left(1 - \exp\left(-x/b\right)\right) \quad (3)$$

In Eq. (3), b is a rate parameter. In order to compute the vigor for each saccade, we follow two steps. Initially, we use a development set with saccades from different subjects (for more information on the development and evaluation sets see Section 4.1), and for each subject we fit Eq. (3) to the saccadic data. By averaging the across subject (development set) rate parameter values—calculated via the curve fitting—we estimate the final value for b_{avg}. Then, we can solve Eq. (3) to estimate the vigor of each individual saccade j made by a subject i (evaluation set), as follows:

$$a_i^j = v^{peak\ j}_i \Big/ \left(1 - \exp\left(-amp_i^j / b_{avg}\right)\right) \quad (4)$$

The complete vigor feature vector for an eye movement recording from subject i is formed by using the distribution of the vigor values corresponding to the N saccades extracted from the recording: $f_i^{vig} = \left\{a_i^1, a_i^2, ..., a_i^N\right\}$.

The use of the vigor features is expected to provide more robustness across different types of visual stimuli (that induce saccades of different amplitudes) than considering the peak velocity and amplitude separately. An alternative option for providing robustness across different stimuli would be to take the ratio of peak velocity and amplitude. However, modeling of the peak velocity-amplitude relationship using a non-linear formula can provide a more accurate representation, as indicated by previous research studies [Bahill et al. 1975], [Robinson 1964; Zuber, Stark and Cook 1965].

2.2 Modeling of Saccadic Acceleration Features

Saccadic eye movements are executed via the combined application of the agonist-antagonist forces from the oculomotor muscles. Thus, the inspection of the acceleration profile of a saccade can provide valuable information regarding the underlying sources of the applied forces. During the execution of a saccade, eye velocity initially increases (acceleration phase) until it reaches a maximum value (peak velocity), and then, velocity starts decreasing (deceleration phase) until the eye reaches its new position. Although the laws of physics require that the area for the acceleration phase must equal the area for the deceleration phase in the force-time profiles, this does not mean that the two parts of the curve need to mirror each other. For example the force during the deceleration phase can have a smaller magnitude and being applied for a larger duration [Abrams et al. 1989]. To avoid any confusion in the subsequent description, the term 'acceleration profile' refers to the curve containing both the 'acceleration phase' (velocity increasing) and the 'deceleration phase' (velocity decreasing).

The existence of asymmetries in the acceleration profiles has been reported by several studies in the past. In the study of [Thomas 1969], the lack of symmetry was observed in the case of vertical saccades of different directions, compared to the more symmetric form of the horizontal saccades of different directions. The different behavior for the vertical and the horizontal saccades was attributed by the author to the stiffer elasticity of the horizontal recti muscles compared to the composite stiffness of the four muscles involved in the vertical eye rotations. Another important finding of this study was that the acceleration profiles coming from different saccades can be similar in their initial parts but subsequently may diverge. In the work of [Fricker 1971], it was reported that the acceleration phase and the deceleration phase in the acceleration profiles can exhibit small asymmetries, e.g. the peak deceleration was found to be somewhat smaller than the peak acceleration. The work of [Abrams et al. 1989] investigated the dynamic properties of the eye movements with the particular focus on the speed-precision trade-off of the saccadic movements. During the inspection of the acceleration profiles for saccades of different amplitudes, the peak deceleration appeared slightly smaller in magnitude compared to the peak acceleration, and the deceleration part of the curve was slightly skewed towards the end. Furthermore, the work of [Collins et al. 2008] explored the dynamics of saccades during the saccadic adaptation, and the findings of this study showed that it is the decelerating phase that tends to be modified by motor learning.

In the current work, we extracted descriptive characteristics from the acceleration profiles of saccades, and modeled the asymmetries of the acceleration and deceleration phases. In Fig. 2, we present example acceleration profiles for saccades executed by different subjects. The saccades correspond to the same stimulus, i.e. a 'jumping' point of light placed to induce horizontal saccades of approximately 30° (eye moving from -15° to 15°).

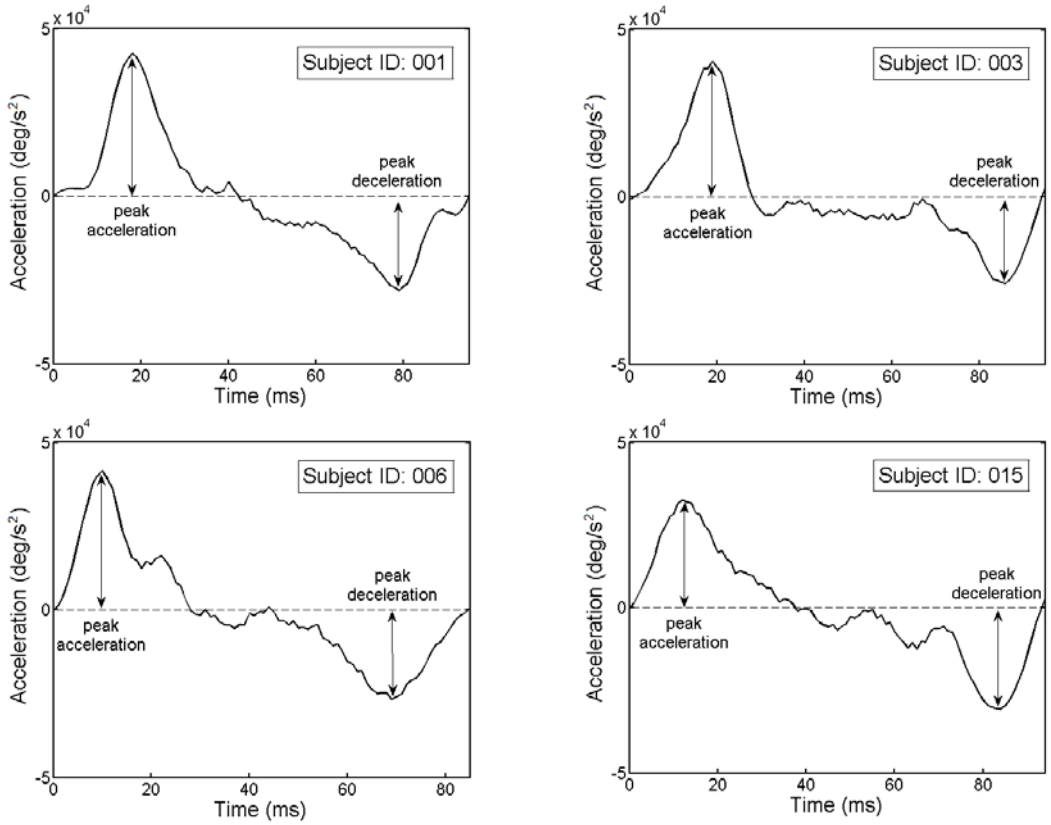

Fig. 2. Presentation of the acceleration profiles for saccades executed by different subjects. Saccades correspond to the same stimulus (point of light), placed to induce horizontal saccades with amplitude of 30° (eye moving from -15° to 15°).

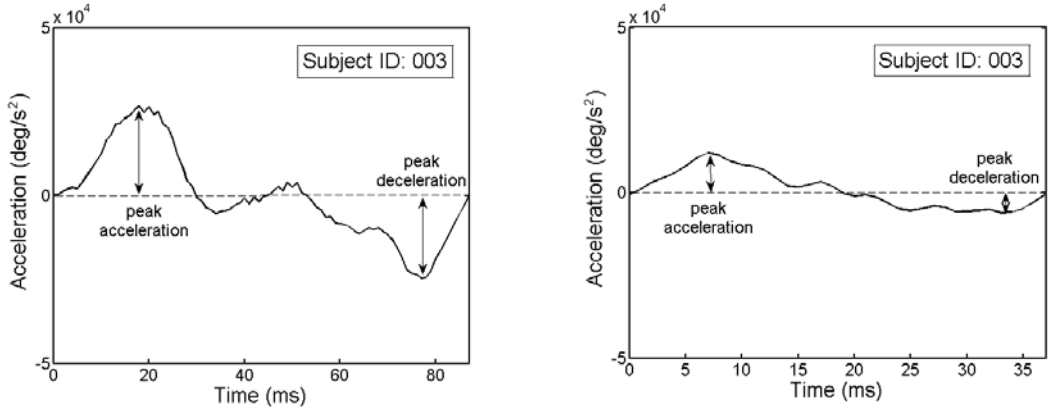

Fig. 3. Presentation of the acceleration profiles for saccades of large and small amplitude executed by the same subject. The first profile (left) corresponds to a saccade of amplitude 20°, and the second (right) to a saccade of amplitude 3°.

An inspection of the acceleration profiles reveals the existence of variations in: a) the overall profile shape, b) the absolute peak values, and c) the ratio of the peak acceleration and peak deceleration values. Apart from the inter-subject differences, there are also variations in the acceleration profiles of saccades coming from the same subject. The exact acceleration values depend on the exact amplitudes of the executed saccades. Saccades of larger amplitudes induce larger peak accelerations and decelerations. In Fig. 3, we show the acceleration profiles for saccades of large and small amplitude coming from the same subject. The goal of our work is to extract the features that emphasize the inter-subject variations with minimum interference from the intra-subject variations.

The procedure for extracting the acceleration features initiates with the calculation of the second derivative from the positional eye movement signal. As in the case of the velocity, we employed the corresponding smoothing second derivative formula suggested by [Bahill and McDonald 1983]. For the calculation of the acceleration for the raw positional sample k and sampling period of T_s, we have:

$$acc(k) = \left(vel\left(k+4\right) - vel\left(k-4\right)\right) \Big/ \left(8 \cdot T_s\right) \tag{5}$$

Then, based on the extracted saccade boundaries by the used classification algorithm (I-VT) we can extract the acceleration profiles for the individual saccades. The proposed features for the representation of the characteristics of the saccadic acceleration profiles are related both to the overall shape of the profile and to the relative difference (ratio) of the peak magnitudes during the acceleration and deceleration phases (accommodating thus for saccades of different amplitudes). Let us denote $acc^{prof\ j}_{\ i}$ the acceleration profile corresponding to a saccade j made by subject i. The first type of features is extracted by calculating the mean activation m_i^j over the entire saccadic acceleration profile, providing an aggregated representation of the means during the acceleration and deceleration phases, i.e. $m^{acc\ j}_{\ i} = \sum_{k=1}^{L} acc^{prof\ j}_{\ i}\left(k\right) \Big/ L$ and $m^{dec\ j}_{\ i} = \sum_{k=L+1}^{K} acc^{prof\ j}_{\ i}\left(k\right) \Big/ K-L-1$, where L are the samples of the acceleration phase and K are the samples representing the whole acceleration profile.

The second type of acceleration features model the relative differences of peak accelerations and decelerations. The peak acceleration ratio for a saccade j made by subject i is calculated as follows:

$$r_i^j = \left|\max_k\left(acc^{prof\ j}_{\ i}\right)\right| \Big/ \left|\min_k\left(acc^{prof\ j}_{\ i}\right)\right| \tag{6}$$

The two types of acceleration feature vectors for a recording coming from subject i are formed using the distributions of all the respective values from the extracted N saccades: $f_i^{acc\_m} = \left\{m_i^1, m_i^2, ..., m_i^N\right\}$ and $f_i^{acc\_r} = \left\{r_i^1, r_i^2, ..., r_i^N\right\}$.

2.3 Incorporation of Features into Complex Eye Movement Behavior Biometrics

During the biometric recognition experiments, the features extracted for vigor f_i^{vig} and acceleration $f_i^{acc\_m}$, $f_i^{acc\_r}$ are integrated into the CEM-B framework [Holland and Komogortsev 2013b]. The employment of the CEM-B framework provides two advantages: a) the easy integration of the new dynamic features as univariate distributions along with the other features of the framework, and b) the possibility for a direct evaluation of the achieved improvement from the integration of the new features compared to the baseline performance of the original features. The extracted features are calculated separately for the horizontal and the vertical components of the eye movement. This modeling leads to a more robust representation of the characteristics of the underlying muscles and neural pulses, given the existing differences in the oculomotor system, previously reported in [Bahill

and Stark 1975]. The effects from these differences are also supported by the observed differences in the profiles of the horizontal and vertical saccades [Collewijn et al. 1988a; Collewijn et al. 1988b].

In Table 1, we present the original CEM-B features and the new proposed features added to the framework. The original CEM-B algorithm extracts a set of 4 fixation and 8 saccade features related to the duration, position, and velocity. With the integration of the new features of saccadic vigor and acceleration the framework will contain a total of 18 features. These features are treated separately as univariate distributions and their comparison can be performed with the use of different distribution similarity measures. In the current work, we use the Two-Sample Kolmogorov-Smirnov test as the preferred distribution comparison measure. During our preliminary experiments we also tested the Two-Sample Cramer-von Mises test but it was found to present equal or inferior performance.

Table 1 Overview of the CEM-B features and the new dynamic features based on saccadic vigor and acceleration.

Original CEM-B features (duration, position, velocity)		**New Dynamic features (vigor, acceleration)**
1. Start time (fixation)	*7. Horizontal amplitude (saccade)*	*13. Horizontal saccadic vigor (saccade)*
2. Duration (fixation)	*8. Vertical amplitude (saccade)*	*14. Vertical saccadic vigor (saccade)*
3. Horizontal centroid (fixation)	*9. Horizontal mean velocity (saccade)*	*15. Horizontal mean acceleration (saccade)*
4. Vertical centroid (fixation)	*10. Vertical mean velocity (saccade)*	*16. Vertical mean acceleration (saccade)*
5. Start time (saccade)	*11. Horizontal peak velocity (saccade)*	*17. Horizontal acceleration ratio (saccade)*
6. Duration (saccade)	*12. Vertical peak velocity (saccade)*	*18. Vertical acceleration ratio (saccade)*

After the comparison phase we end up with 18 similarity matrices containing the pairwise scores from the compared feature vectors. These matrices should be combined in order to generate a single similarity score for each pairwise comparison, which will be used for performing the biometric recognition. In this work, we evaluate four fusion schemes for the combination of the similarity scores: the Simple Mean—or Sum—(SM) [Snelick et al. 2005], the Weighted Mean based on Rank-1 IR performance (WM) [Rigas et al. 2015], the Random Forests (RF) scheme Breiman [2001], and the Likelihood Ratio (LR) scheme [Nandakumar et al. 2008]. For training the parameters of the WM, RF, and LR fusion algorithms we used the development dataset (see Section 4.1). In Fig.4, we provide a schematic diagram summarizing the procedures followed for the extraction of the saccadic vigor and acceleration features, and their incorporation into the CEM-B framework for performing the task of biometric recognition.

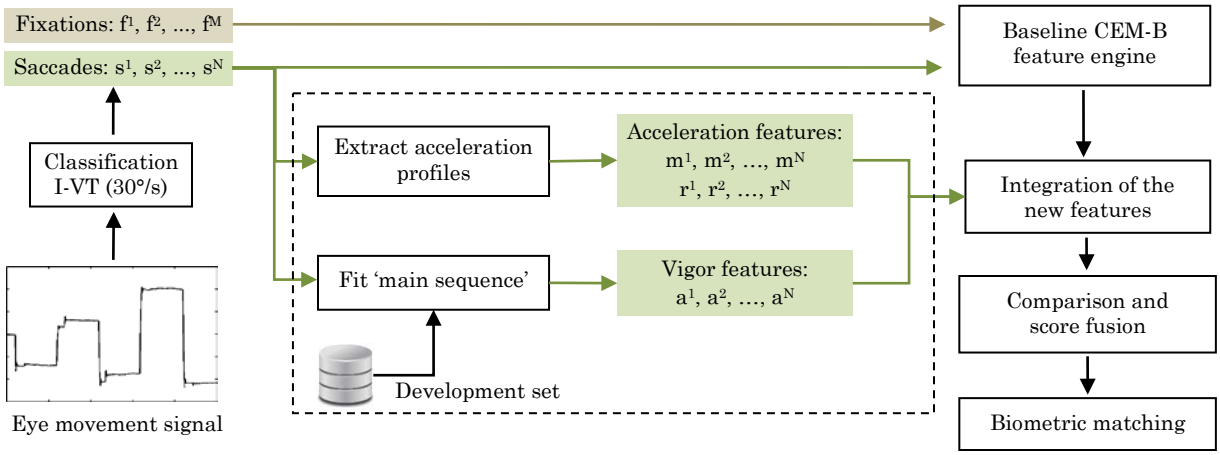

Fig. 4. Diagram of the procedures for the integration of saccadic vigor and acceleration features into the CEM-B framework.

3. EXPERIMENTS

3.1 Apparatus

The used eye-tracking device was an SR Research EyeLink 1000 eye-tracker [EyeLink], working at 1000 Hz. During the experiments, the measured average calibration accuracy was 0.49° (SD = 0.17°), and the average data validity was 96.8% (SD = 4.9%). The calibration accuracy was calculated via the measurement of the error of the eye landing positions compared to the expected positions of the calibration points (9 points were used in our experiments). The data validity was calculated via the measurement of the total percent of samples that the eye-tracker was not able to capture successfully, e.g. due to blinking, moisture, squinting etc. Furthermore, we used artificial eyes provided by SR Research to measure the eye-tracking precision (noise), which was found to be 0.034° (SD = 0.006°).

The visual stimuli were presented on a flat screen monitor with dimensions of 474 × 297 mm and resolution of 1680 × 1050 pixels, placed at a distance of 550 mm from the subject. To ensure the maximum quality of the recorded data we used a chinrest with a head bar to stabilize subject's head.

3.2 Participants

The experiments were conducted with 322 subjects (171 male/151 female), ages 18-46 (M = 22, SD = 4.2). From those subjects, 163 had a corrected vision (67 glasses/96 contact lenses). The subjects performed 2 recording sessions each, separated by a time interval of approximately 20 minutes for each visual stimulus, leading to the collection of 1866 unique recordings. Texas State University's institutional review board approved the study, and every subject provided informed consent.

3.3 Visual Stimulus

The visual stimuli were chosen to induce saccades of various amplitudes, peak velocities, and accelerations, allowing thus for the evaluation of the saccadic vigor and acceleration cues. The adopted visual stimuli were the following:

Random 'Jumping' Point (RAN): this stimulus consisted of a point (white circle with a black center) appearing at random positions in the black background of a computer screen. The point changed position every 1 second, and the duration of each experimental trial was 1 minute and 40 seconds. The specific stimulus induces random oblique saccades of different amplitudes.

Text Excerpts (TEX): the participants read freely some text excerpts from the poem of Lewis Carroll 'The Hunting of the Snark'. The total time that was given to the participants to read the excerpts was 1 minute. For the specific stimulus, the amplitudes of the saccades are not totally random but they can form patterns according to the reading behaviors of the subjects.

Video Sequence (VID): the participants watched freely a part from the video trailer of the Hollywood movie 'The Hobbit: The Desolation of Smaug'. The total duration of the video sequence was 1 minute. For the specific stimulus the subjects perform more complex patterns of fixations and saccades (and occasionally smooth pursuits) as they observe the dynamically changing video content.

Recordings for RAN, TEX and VID stimuli were a part of a larger experiment where subjects performed various eye movement tasks with several periods of rest to reduce possible fatigue effects. Total duration of all tasks and periods of rest did not exceed 1 hour.

4. RESULTS

4.1 Evaluation Procedure

In our experiments we split the data into development and evaluation datasets using 20 random partitions and with a subject ratio of 50%-50% (the subjects of the development and evaluation sets did not overlap, to avoid any overfitting effects). In each case, the data from the development set were

used to train the algorithms' parameters (see Section 2.1 and Section 2.3), and the data from the evaluation set were used for the calculation of the performance rates presented below. All the reported rates were calculated by averaging the results over the 20 partitions.

For the evaluation of biometric verification and identification performance we use the following measures:

Equal Error Rate (EER): The EER is a measure of the verification performance of a biometric system. A genuine score is defined as the score from the comparison of biometric samples from the same identity. An impostor score is defined as the score from the comparison of biometric samples from different identities. By defining an acceptance threshold (η) we can compute the False Rejection Rate (FRR) as the percentage of the genuine scores that fall under the threshold η, and the False Acceptance Rate (FAR) as the percentage of the impostor scores that are over η. The True Positive Rate (TPR) can be defined as the percentage of genuine scores that are over the threshold η, and it stands TPR = 1 - FRR. By changing the acceptance threshold we can construct a Receiver Operating Characteristic (ROC) curve and calculate the EER as the point of operation where the FRR equals the FAR. For the construction of the ROC curves we employed the technique of vertical averaging [Fawcett 2006] over the 20 partitions.

Rank-1 Identification Rate (Rank-1 IR): The Rank-k Identification Rate (Rank-k IR) is a measure of the biometric identification performance which shows the percentage of genuine scores that can be found within the k top places of a ranked list. A Cumulative Match Characteristic (CMC) curve shows the change of the identification rate as a function of the used rank k. The Rank-1 IR is defined as the percent of biometric samples with a correct match in the first place of the ranked list.

4.2 Biometric Recognition Performance

In this section, we evaluate the biometric performance that can be achieved from the integration of the saccadic vigor and acceleration features in the original CEM-B framework. For these experiments we use the Simple Mean (SM) as a common scheme for fusion in all tested cases. In Section 4.3, we additionally show the performances that can be achieved when using the other fusion schemes (WM, RF, LR). In Fig. 5 and Fig. 6 we present the achieved EER and Rank-1 IR performances for each type of visual stimulus in the form of bar diagrams with error bars showing the error margins in 95% confidence interval. For a comprehensive presentation of the relative improvement offered by the vigor and acceleration features we show the results in the following four cases: 1) C1: the baseline performance of the original CEM-B framework, 2) C2: the improvement offered by the incorporation of the vigor features alone, 3) C3: the improvement offered by the incorporation of acceleration features alone, and 4) C4: the finally achieved improvement by the incorporation of both types of features. It should be emphasized that during our experiments we used exactly the same settings (comparison/fusion scheme etc.) for the four cases in order to ensure a fair comparison.

In the *verification scenario* for the *RAN stimulus* (Fig. 5-left) the baseline EER (C1) is 17.92%. The incorporation of the vigor (C2) and the acceleration (C3) features separately improves the EER to 14.97% and 13% accordingly. The integration of both types of features (C4) leads to the final EER of 11.92%. For evaluating the significance of the improvements we performed pairwise one-way ANOVAs across the four cases in the order of successive improvement, using the values from the 20 random partitions. The differences in performance were found to be statistically significant in all cases. For the pair C1-C2 we had $F_{(1, 38)} = 92.61$, $p < 0.001$, for the pair C2-C3 $F_{(1, 38)} = 42.18$, $p < 0.001$, and for the pair C3-C4 $F_{(1, 38)} = 9.63$, $p < 0.01$. In the *identification scenario* for the *RAN stimulus* (Fig.6-left) the baseline Rank-1 IR (C1) is 34.41%, and with the incorporation of the vigor features (C2) it improves to 44.02%, whereas with the incorporation of the acceleration features (C3) it improves to 48.59%. The integration of both types of features (C4) leads to the final Rank-1 IR of 55.56%. The pairwise one-way ANOVAs reveal that the differences are statistically significant in all cases, and

specifically, for the pair C1-C2 $F_{(1, 38)} = 166.44$, $p < 0.001$, for the pair C2-C3 $F_{(1, 38)} = 34.9$, $p < 0.001$, and for the pair C3-C4 $F_{(1, 38)} = 86.32$, $p < 0.001$.

In the *verification scenario* for the *TEX stimulus* (Fig. 5-middle) the baseline value for the EER (C1) is 14.61%. The incorporation of the vigor (C2) and the acceleration (C3) features separately improves the EER to 12.45% and 10.64%. Finally, the integration of both features (C4) improves the EER to 9.57%. The pairwise one-way ANOVAs reveal a significant main effect for the pair C1-C2 with $F_{(1, 38)} = 61.74$, $p < 0.001$, for the pair C2-C3 with $F_{(1, 38)} = 28.45$, $p < 0.001$, and for the pair C3-C4 with $F_{(1, 38)} = 9.03$, $p < 0.01$. In the case of the *identification scenario* for the TEX stimulus (Fig. 6-middle) the baseline Rank-1 IR (C1) is 52.58%. With the incorporation of the vigor features (C2) the Rank-1 IR improves to 56.34%, and with the incorporation of the acceleration features (C3) it improves to 60.65%. The final value of Rank-1 IR after the integration of both features (C4) is 64.29%. The pairwise one-way ANOVAs reveal that all the differences are statistically significant, with the respective values for the pair C1-C2 $F_{(1, 38)} = 21.39$, $p < 0.001$, for the pair C2-C3 $F_{(1, 38)} = 29.01$, $p < 0.001$, and for the pair C3-C4 $F_{(1, 38)} = 18.26$, $p < 0.001$.

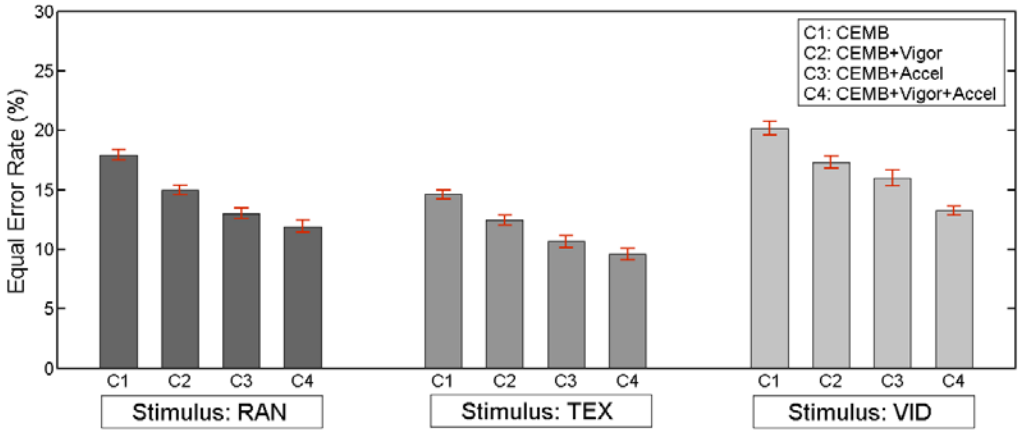

Fig. 5. The EER performances for the different types of visual stimulus.

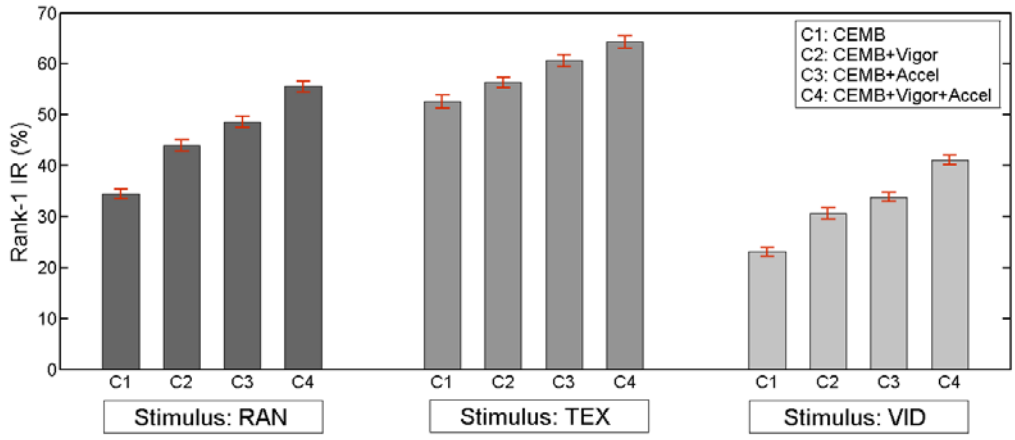

Fig. 6. The Rank-1 IR performances for the different types of visual stimulus.

In the *verification scenario* for the *VID stimulus* (Fig. 5-right) the EER of the baseline CEM-B (C1) is 20.17%. The incorporation of the vigor features (C2) improves EER to 17.30%, and the incorporation of the acceleration features (C3) improves EER further down to 15.99%. The joint integration of the vigor and the acceleration features (C4) leads to the final EER of 13.23%. The pairwise one-way ANOVAs across the 20 random partitions showed a statistical significant difference in all the tested

cases. For the pair C1-C2 we had $F_{(1, 38)} = 52.42$, $p < 0.001$, for the pair C2-C3 $F_{(1, 38)} = 9.43$, $p < 0.01$, and for the pair C3-C4 $F_{(1, 38)} = 48.21$, $p < 0.01$. In the *identification scenario* for the *VID stimulus* (Fig.6-right) the baseline Rank-1 IR (C1) has a value of 23.07%. With the incorporation of the vigor features (C2) the Rank-1 IR increases to 30.63%, and with the incorporation of the acceleration features (C3) it improves to 33.87%. The integration of both types of features (C4) leads to the final Rank-1 IR of 41.10%. The pairwise one-way ANOVAs demonstrate the statistical significance of the reported differences for the pair C1-C2 $F_{(1, 38)} = 106.95$, $p < 0.001$, for the pair C2-C3 $F_{(1, 38)} = 19.48$, $p < 0.001$, and for the pair C3-C4 $F_{(1, 38)} = 111.3$, $p < 0.001$.

The EER and the Rank-1 IR are compact measures that can summarize the verification and the identification performance of a biometric recognition system. We also present the ROC and CMC curves, in order to provide a more global overview of the variation of the biometric recognition rates when changing the sensitivity of the system. In Fig. 7, we show the ROC curve clusters for the four evaluated cases (C1-C4) and for each type of visual stimulus separately. Similarly, in Fig. 8 we present the CMC curve clusters for the respective cases. The diagrams allow for a generalized assessment of the relative improvement of the baseline scheme (C1) both when we integrate vigor or acceleration features separately (C2, C3), and when we integrate both feature types (C4).

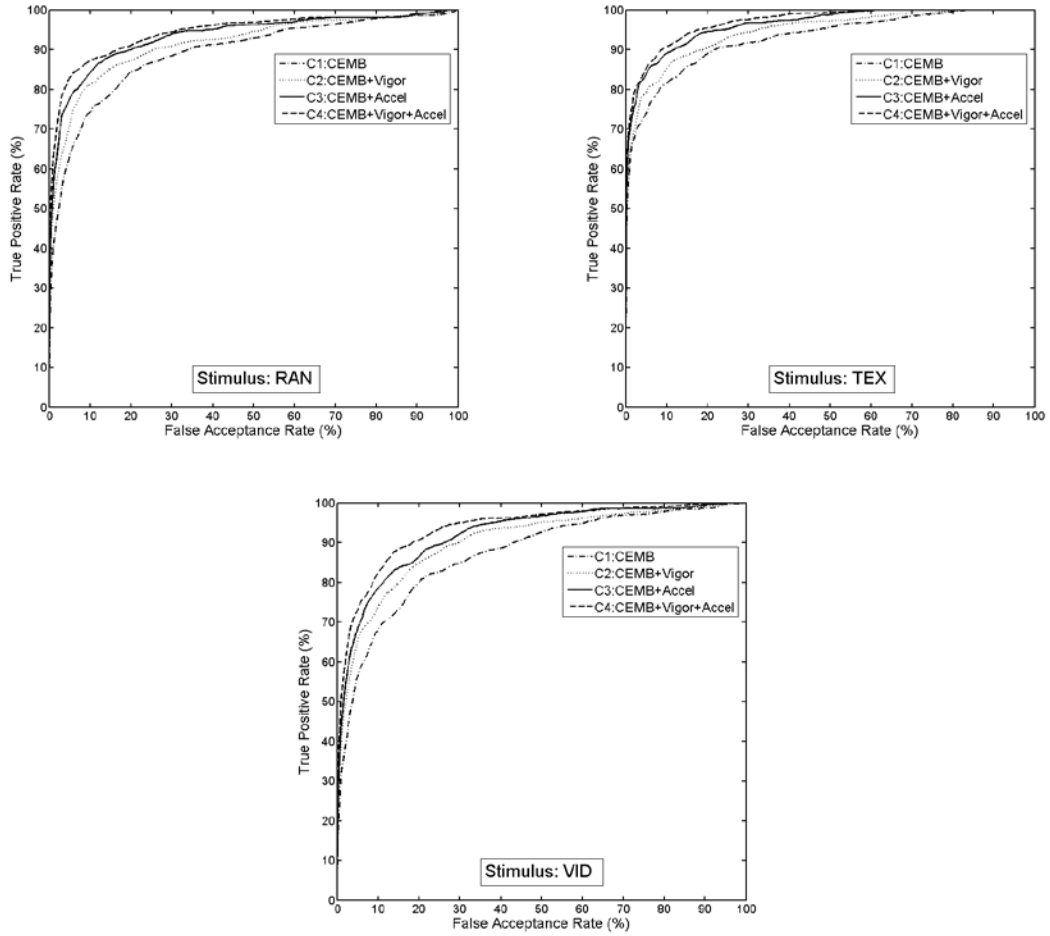

Fig. 7. The constructed ROC curves demonstrating the overall performance in the verification scenario for the different types of visual stimulus.

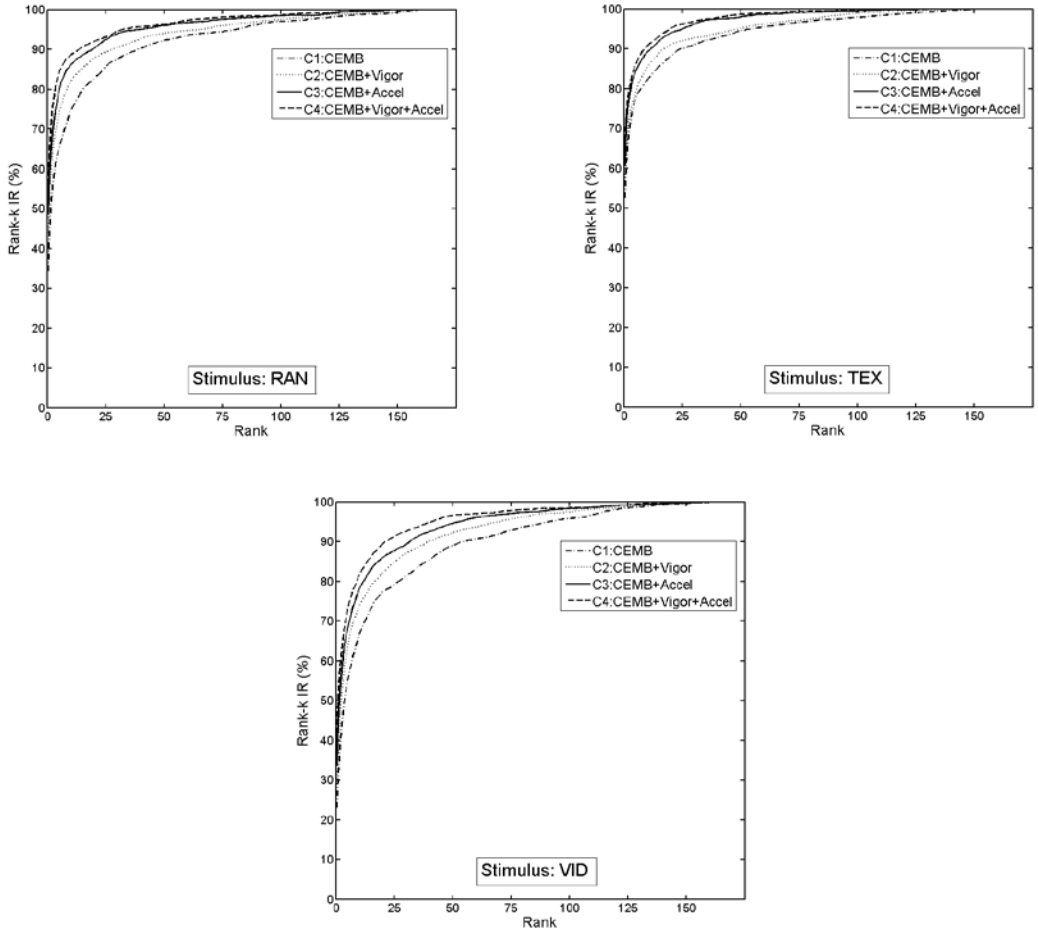

Fig. 8. The constructed CMC curves demonstrating the overall performance in the identification scenario for the different types of visual stimulus.

4.3 Analysis of the Fusion Schemes

In this section, we provide a comparative presentation of the achieved biometric performances when employing different schemes for performing fusion in the comparison score level. In Tables 2, 3, and 4 we present the calculated values for the EER and Rank-1 IR for the RAN, TEX, and VID stimuli respectively. An overview of the achieved rates reveals moderate performance differentiations of the employed fusion schemes. The weighted mean (WM) fusion scheme provides the optimum overall rates, however, the other schemes can also achieve competitive rates on several occasions. In order to examine the statistical significance of these differences we report below the results of the performed ANOVA analyses across selected fusion schemes, using the data from the 20 random partitions. In these analyses we examine only the final case (C4), i.e. after the integration of both vigor and acceleration features, since it yields the finally achieved best recognition rates.

An inspection of the fusion scheme comparison results for the RAN stimulus (Table 2) reveals that in this case three of the fusion schemes (SM, WM, LR) yield similar performances whereas the RF fusion scheme performs worse than the others. In this case, the one-way ANOVA across all schemes reveals a statistically significant main effect, $F_{(3, 76)} = 23.46$, $p < 0.001$. The exclusive comparison of the top two performing schemes (WM, LR), though, does not reveal a strong effect, $F_{(1, 38)} = 3.18$, $p = 0.08$.

For the case of Rank-1 IR the difference is statistically significant both across all schemes $F_{(3, 76)} = 54.4$, $p < 0.001$, and between the top two performing schemes (WM, SM) $F_{(1, 38)} = 14.79$, $p < 0.001$.

The fusion scheme comparison results for the TEX stimulus (Table 3) reveal again a moderate superiority of the WM scheme over the others. This difference in performance is found to be statistically significant both across all fusion schemes, $F_{(3, 76)} = 10.46$, $p < 0.001$, and during the exclusive comparison of the top two performing schemes (WM, RF) $F_{(1, 38)} = 9.11$, $p < 0.01$. For the case on Rank-1 IR, the relatively lower performance of the LR scheme induces a significant main effect across all schemes $F_{(3, 76)} = 67.55$, $p < 0.001$, however, the comparison of the top two performing schemes (WM, RF) does not show a strong statistical difference $F_{(1, 38)} = 3.12$, $p = 0.08$.

The biometric performance rates for the VID stimulus presented in Table 4 show that in this case the effects of the different fusion schemes are even less pronounced. The results of the one-way ANOVA for the EER show a significant main effect across all fusion schemes $F_{(3, 76)} = 51.63$, $p < 0.001$, however, there is no significant main effect across the top two performing schemes (WM, LR) $F_{(1, 38)} = 0.01$, $p = 0.93$. The same results hold for the case of the Rank-1 IR where the across fusion scheme effect was significant $F_{(3, 76)} = 59.65$, $p < 0.001$, but the top two performing schemes (WM, SM) did not show a significant difference $F_{(1, 38)} = 0.33$, $p = 0.57$.

Table 2 Comparison of the different fusion schemes for the RAN stimulus.

Stimulus: RAN								
Case	**EER (SD) %**				**Rank-1 IR (SD) %**			
	SM	***WM***	***RF***	***LR***	***SM***	***WM***	***RF***	***LR***
C1	17.92 (1.01)	16.46 (0.99)	20.20 (1.09)	16.83 (1.02)	34.41 (2.25)	38.21 (1.94)	29.75 (2.51)	34.58 (2.19)
C2	14.70 (0.92)	13.26 (1.01)	15.81 (1.13)	13.89 (0.98)	44.02 (2.46)	48.93 (2.55)	41.97 (3.44)	46.01 (2.24)
C3	13.00 (0.99)	12.11 (1.24)	15.83 (0.89)	12.68 (0.98)	48.59 (2.43)	51.51 (2.69)	39.97 (2.28)	45.87 (2.01)
C4	11.91 (1.20)	10.95 (1.02)	13.71 (1.03)	11.55 (1.13)	55.56 (2.31)	58.49 (2.51)	47.89 (3.20)	54.11 (2.74)

Table 3 Comparison of the different fusion schemes for the TEX stimulus.

Stimulus: TEX								
Case	**EER (SD) %**				**Rank-1 IR (SD) %**			
	SM	***WM***	***RF***	***LR***	***SM***	***WM***	***RF***	***LR***
C1	14.61 (0.84)	11.87 (0.80)	12.72 (1.08)	13.08 (0.84)	52.58 (2.74)	54.46 (2.64)	53.88 (3.40)	44.77 (2.75)
C2	12.45 (0.90)	9.51 (0.85)	9.90 (0.84)	10.06 (0.91)	56.34 (2.38)	60.40 (2.49)	60.11 (3.47)	47.81 (3.16)
C3	10.64 (1.21)	8.62 (0.89)	10.69 (1.17)	10.89 (0.69)	60.65 (2.68)	63.52 (2.60)	60.34 (3.09)	52.78 (2.90)
C4	9.57 (1.04)	8.12 (0.86)	8.88 (0.72)	9.13 (0.68)	64.29 (2.70)	66.63 (3.03)	64.69 (3.87)	53.80 (2.87)

Table 4 Comparison of the different fusion schemes for the VID stimulus.

Stimulus: VID								
Case	**EER (SD) %**				**Rank-1 IR (SD) %**			
	SM	***WM***	***RF***	***LR***	***SM***	***WM***	***RF***	***LR***
C1	20.17 (1.36)	19.39 (1.33)	22.95 (1.58)	18.82 (1.34)	23.07 (2.05)	27.70 (2.99)	27.11 (1.97)	21.43 (1.58)
C2	17.30 (1.14)	14.67 (1.24)	18.63 (1.04)	15.01 (1.52)	30.64 (2.55)	34.57 (2.30)	32.76 (2.48)	28.39 (2.17)
C3	15.99 (1.53)	15.14 (1.40)	18.82 (1.30)	14.65 (1.27)	33.87 (2.06)	37.64 (1.94)	37.24 (1.98)	28.21 (3.11)
C4	13.23 (0.91)	13.13 (0.92)	17.05 (1.57)	13.17 (1.30)	41.10 (2.28)	41.55 (2.64)	40.20 (2.31)	31.91 (3.22)

5. DISCUSSION

5.1 The Effects on Performance

Our main goal was to investigate the extent of improvement that can be achieved by incorporating information about saccadic vigor and acceleration in an eye movement biometric framework. We found that the addition of these features can improve the biometric accuracy considerably. The complete extent of the achieved improvement can be quantified in terms of the relative improvement of the final performance (C4) compared to the baseline case (C1). For the case of the verification scenario (EER), the performance for the RAN stimulus improved by 33.5%, the performance for the TEX stimulus improved by 31.6%, and the performance for the VID stimulus improved by 32.3%. For the identification scenario the relative improvement of Rank-1 IR was even more pronounced, as the performance improved by 53.1% for the RAN stimulus, by 22.3% for the TEX stimulus, and by 50% for the VID stimulus. Therefore, these results suggest that the addition of vigor and acceleration features can yield a considerable advance both for the baseline performance of the original CEM-B framework and for the field of eye movement biometrics in general.

The improvement in performance was also notable when incorporating each of the proposed features (vigor, acceleration) separately. Specifically, incorporating the vigor features (C2) alone brought about a relative decrease in the EER rates by 19.4% (RAN), 19.9% (TEX), and 24.3% (VID), and a relative increase in Rank-1 IR rates by 28% (RAN), 10.9% (TEX), and 24.8% (VID). Analogously, when incorporating only the acceleration features (C3) there was a relative decrease in the EER rates by 26.4% (RAN), 27.4% (TEX), and 21.6% (VID), and an increase in the Rank-1 IR rates by 34.8% (RAN), 16.6% (TEX), and 35.9% (VID). These results underline the relevance of each of the newly proposed features (vigor, acceleration), and more importantly they show that the performance of the one feature-type does not negate the performance of the other during their common integration into the baseline biometric framework.

During our analysis we also experimented with different fusion schemes for the combination of information coming from the different features. The evaluated schemes performed with similar rates, with the WM scheme showing the best performance and the most stable behavior. The other schemes interchanged their roles at the second place for the three types of visual stimulus. Furthermore, the VID stimulus seems to be less affected by the selection of a specific fusion scheme. Given the obtained results and considering the increased computational complexity of the more sophisticated fusion schemes (RF, LR), the WM scheme (or alternatively the SM scheme) appears as the preferred choice for the biometric recognition scenario.

5.2 The Effects of Different Visual Stimuli

One objective of our research was to specifically inspect the impact in performance of the newly proposed features when using different types of visual stimulus. The results revealed that the relative improvement in performance was more emphasized for the cases of the RAN and the VID stimuli, whereas the relative improvement for the TEX stimulus was in most cases the least among the three types. This result, partially confirms our hypothesis that the proposed features can provide a more sophisticated modeling of the relationships between the amplitude, peak velocity, and acceleration of the saccades. For example, in the case of the RAN and the VID stimuli the variety in the generated saccadic amplitudes is larger, and can therefore justify the greater improvement in performance (almost doubling for Rank-1 IR). In the case of the TEX stimulus the variety of the saccadic amplitudes can be limited due to the reading pattern layout. It should be noted that the relatively smaller improvement for the TEX stimulus can be also partially attributed to the fact that the performances for the other two types of stimulus start from a worse baseline, leaving thus a larger margin for improvement.

5.3 Practical Applicability Considerations

During the implementation of the experimental recordings we employed a high-grade eye-tracking device and we stabilized the subjects' heads in order to ensure the highest possible data quality. It should be noted, though, that during a practical (out-of-the-lab) implementation of a biometric recognition system, several factors can interfere with the capturing procedure, such as the unconstrained (free) head movements, the variable lighting conditions (inducing variability in the pupil size), and the environmental noise. The advances of the eye-tracking technology in recent years, move towards the mitigation of such effects, e.g. via the development of robust remote and wearable solutions [SMI 2015; THEEYETRIBE 2015; Tobii 2015] that can perform eye-tracking with acceptable quality in less than ideal conditions. Furthermore, previous research [Holland and Komogortsev 2013a] has shown that the performance loss for eye movement-driven biometrics remains in acceptable levels for specifications of minimum sampling rate of 250 Hz, eye-tracking precision better (lower) than 0.5°, and maximum allowed calibration error lower than 1.5°.

The eye movements require a prolonged recording time compared to the static biometric features like the iris and the fingerprints. This inherent limitation of the eye movements can be counterbalanced by the provided counterfeit resistance properties, and also, by the given opportunity to build applications for the task of continuous verification [Niinuma et al. 2010]. Another urging investigation related to the practical adoption of the eye movement biometrics regards the reliability of the extracted features under physical and behavioral changes of the user (as well as of his/her co-operation). Previous research shows that some eye movement characteristics can be influenced by several conditions, such as user fatigue [Abdulin and Komogortsev 2015], anxiety [Miltner et al. 2004], and intoxication [Nawrot et al. 2004]. Also, the results of preliminary research show that the recording time intervals can induce template aging effects, which can also affect the biometric performance [Komogortsev et al. 2014a]. A comprehensive exploration of such limitations and practical considerations is very important for the future adoption of the eye movement biometrics, since it would allow for the discovery of the features that can provide the optimal operational conditions in a real-world biometric scenario.

6. CONCLUSION

In this work, we utilized saccadic eye movements of over 300 individuals for the extraction of saccadic vigor and acceleration features, and then, we incorporated the extracted features into an eye movement-driven biometric framework. Our findings support that the incorporation of the proposed features can lead to an increase in the biometric accuracy, and improve the robustness when using different types of visual stimulus. In the future, we plan to investigate additional schemes for modeling the eye movement features based on findings related to the physiological connections between the eye movements and the brain functionality. Also, it should be noted that the current work explored only saccadic and fixational features of the eye movements, even in the case when smooth pursuit movements were exhibited in response to the video stimulus. In future research we intend to explore the properties of the smooth pursuit movements to improve the accuracy and robustness of the ocular biometrics framework.

REFERENCES

ABDULIN, E. and KOMOGORTSEV, O. 2015. User Eye Fatigue Detection via Eye Movement Behavior. In *Proceedings of the 33rd Annual ACM Conference Extended Abstracts on Human Factors in Computing Systems*2015 ACM, 1265-1270.

ABRAMS, R.A., MEYER, D.E. and KORNBLUM, S. 1989. Speed and accuracy of saccadic eye movements: characteristics of impulse variability in the oculomotor system. *J. Exp Psychol Hum Percept Perform 15*, 529-543.

BAHILL, A.T., CLARK, M.R. and STARK, L. 1975. The main sequence, a tool for studying human eye movements. *Mathematical Biosciences 24*, 191-204.

BAHILL, A.T. and MCDONALD, J.D. 1983. Frequency Limitations and Optimal Step Size for the Two-Point Central Difference

Derivative Algorithm with Applications to Human Eye Movement Data. *IEEE Transactions on Biomedical Engineering BME-30*, 191-194.
BAHILL, A.T. and STARK, L. 1975. Neurological control of horizontal and vertical components of oblique saccadic eye movements. *Mathematical Biosciences 27*, 287-298.
BAHILL, T.A., BROCKENBROUGH, A. and TROOST, B.T. 1981. Variability and development of a normative data base for saccadic eye movements. *Invest Ophthalmol Vis, Sci 21*, 116-125.
BALOH, R.W., SILLS, A.W., KUMLEY, W.E. and HONRUBIA, V. 1975. Quantitative measurement of saccade amplitude, duration, and velocity. *Neurology 25*, 1065-1070.
BEDNARIK, R., KINNUNEN, T., MIHAILA, A. and FRÄNTI, P. 2005. Eye-Movements as a Biometric. In *Image Analysis*, H. KALVIAINEN, J. PARKKINEN and A. KAARNA Eds. Springer Berlin Heidelberg, 780-789.
BOLLEN, E., BAX, J., VAN DIJK, J.G., KONING, M., BOS, J.E., KRAMER, C.G.S. and VAN DER VELDE, E.A. 1993. Variability of the main sequence. *Invest Ophthalmol Vis, Sci 34*, 3700-3704.
BREIMAN, L. 2001. Random Forests. *Machine Learning 45*, 5-32.
BUSWELL, G.T. 1935. *How People Look at Pictures: a Study of the Psychology of Perception in Art* The University of Chicago Press, Chicago, IL.
CANTONI, V., GALDI, C., NAPPI, M., PORTA, M. and RICCIO, D. 2015. GANT: Gaze analysis technique for human identification. *Pattern Recognition 48*, 1027-1038.
CARLTON, L.G. and NEWELL, K.M. 1988. Force variability and movement accuracy in space-time. *Journal of Experimental Psychology: Human Perception and Performance 14*, 24-36.
CHOI, J.E.S., VASWANI, P.A. and SHADMEHR, R. 2014. Vigor of Movements and the Cost of Time in Decision Making. *The Journal of Neuroscience 34*, 1212-1223.
CIFU, D.X., WARES, J.R., HOKE, K.W., WETZEL, P.A., GITCHEL, G. and CARNE, W. 2015. Differential eye movements in mild traumatic brain injury versus normal controls. *J Head Trauma Rehabil. 30*, 21-28.
COLLEWIJN, H., ERKELENS, C.J. and STEINMAN, R.M. 1988a. Binocular co-ordination of human horizontal saccadic eye movements. *Journal of Physiology 404*, 157-182.
COLLEWIJN, H., ERKELENS, C.J. and STEINMAN, R.M. 1988b. Binocular co-ordination of human vertical saccadic eye movements. *Journal of Physiology 404*, 183-197.
COLLINS, T. and DORÉ-MAZARS, K. 2006. Eye movement signals influence perception: evidence from the adaptation of reactive and volitional saccades. *Vision Res. 46*, 3659-3673.
COLLINS, T., SEMROUD, A., ORRIOLS, E. and DORÉ-MAZARS, K. 2008. Saccade Dynamics before, during, and after Saccadic Adaptation in Humans. *Invest. Ophthalmol. Vis. Sci. 49*, 604-612.
DI STASI, L.L., ANTOLÍ, A. and CAÑAS, J.J. 2011. Main sequence: An index for detecting mental workload variation in complex tasks. *Applied Ergonomics 42*, 807-813.
ECKSTEIN, M.P., BEUTTER, B.R., PHAM, B.T., SHIMOZAKI, S.S. and STONE, L.S. 2007. Similar Neural Representations of the Target for Saccades and Perception during Search. *The Journal of Neuroscience 27*, 1266-1270.
EYELINK EyeLink 1000 Eye Tracker.
FAWCETT, T. 2006. An introduction to ROC analysis. *Pattern Recognition Letters 27*, 861-874.
FRICKER, S.J. 1971. Dynamic measurements of horizontal eye motion. I. Acceleration and velocity matrices. *Invest Ophthalmol. 10*, 724-732.
GOOGLE Google Glass.
HAITH, A.M., REPPERT, T.R. and SHADMEHR, R. 2012. Evidence for hyperbolic temporal discounting of reward in control of movements. *J Neurosci. 32*, 11727-11736.
HOLCOMB, J.H., HOLCOMB, H.H. and DE LA PENA, A. 1977. Selective attention and eye movements while viewing reversible figures. *Percept Mot Skills 44*, 639-644.
HOLLAND, C.D. and KOMOGORTSEV, O.V. 2013a. Complex Eye Movement Pattern Biometrics: The Effects of Environment and Stimulus. *IEEE Transactions on Information Forensics and Security 8*, 2115-2126.
HOLLAND, C.D. and KOMOGORTSEV, O.V. 2013b. Complex eye movement pattern biometrics: Analyzing fixations and saccades. In *2013 International Conference on Biometrics (ICB)*, 1-8.
IKEDA, T. and HIKOSAKA, O. 2007. Positive and negative modulation of motor response in primate superior colliculus by reward expectation. *J Neurophysiol. 98*, 3163-3170.
JAVAL, E. 1878. Essai sur la physiologie de la lecture. *Annales d'Oculistique (79), 97-117, (80), 135-147, 240-274.*
JUST, M.A. and CARPENTER, P.A. 1980. A theory of reading: from eye fixations to comprehension. *Psychol Rev 87*, 329-354.
KASPROWSKI, P. and OBER, J. 2004. Eye Movements in Biometrics. In *Biometric Authentication*, D. MALTONI and A.K. JAIN Eds. Springer Berlin Heidelberg, 248-258.
KINNUNEN, T., SEDLAK, F. and BEDNARIK, R. 2010. Towards task-independent person authentication using eye movement signals. In *Proceedings of the 2010 Symposium on Eye-Tracking Research & Applications*2010 ACM, 187-190.
KOMOGORTSEV, O., HOLLAND, C., KARPOV, A. and PRICE, L.R. 2014b. Biometrics via Oculomotor Plant Characteristics: Impact of Parameters in Oculomotor Plant Model. *ACM Trans. Appl. Percept. 11*, 1-17.
KOMOGORTSEV, O.V. and HOLLAND, C.D. 2014. The application of eye movement biometrics in the automated detection of mild traumatic brain injury. In *Proceedings of the 32nd Annual ACM Conference on Human Factors in Computing Systems*2014 ACM, 1711-1716.
KOMOGORTSEV, O.V., HOLLAND, C.D. and KARPOV, A. 2014a. Template aging in eye movement-driven biometrics. In

SPIE, Biometric and Surveillance Technology for Human and Activity Identification XI, 90750A-90750A-90759.
KOMOGORTSEV, O.V., KARPOV, A. and HOLLAND, C.D. 2015. Attack of Mechanical Replicas: Liveness Detection With Eye Movements. *IEEE Transactions on Information Forensics and Security 10*, 716-725.
KOMOGORTSEV, O.V., KARPOV, A., HOLLAND, C.D. and PROENCA, H.P. 2012b. Multimodal ocular biometrics approach: A feasibility study. In *IEEE Fifth International Conference on Biometrics: Theory, Applications and Systems (BTAS)*, 209-216.
KOMOGORTSEV, O.V., KARPOV, A., PRICE, L.R. and ARAGON, C. 2012a. Biometric authentication via oculomotor plant characteristics. In *5th IAPR International Conference on Biometrics (ICB)*, 413-420.
KOWLER, E., ANDERSON, E., DOSHER, B. and BLASER, E. 1995. The role of attention in the programming of saccades. *Vision Res. 35*, 1897-1916.
LEIGH, R.J. and ZEE, D.S. 2006. *The Neurology of Eye Movements*. Oxford University Press.
MARCEL, S., NIXON, M.S. and LI, S.Z. 2014. *Handbook of Biometric Anti-Spoofing: Trusted Biometrics under Spoofing Attacks*. Springer Publishing Company, Incorporated.
MILTNER, W.H.R., KRIESCHEL, S., HECHT, H., TRIPPE, R. and WEISS, T. 2004. Eye movements and behavioral responses to threatening and nonthreatening stimuli during visual search in phobic and nonphobic subjects. *Emotion 4*, 323-339.
NANDAKUMAR, K., YI, C., DASS, S.C. and JAIN, A.K. 2008. Likelihood Ratio-Based Biometric Score Fusion. *IEEE Transactions on Pattern Analysis and Machine Intelligence 30*, 342-347.
NAWROT, M., NORDENSTROM, B. and OLSON, A. 2004. Disruption of eye movements by ethanol intoxication affects perception of depth from motion parallax. *Psychol Sci. 15*, 858-865.
NIINUMA, K., UNSANG, P. and JAIN, A.K. 2010. Soft Biometric Traits for Continuous User Authentication. *IEEE Transactions on Information Forensics and Security 5*, 771-780.
NOTON, D. and STARK, L. 1971a. Scanpaths in eye movements during pattern perception. *Science (New York, N.Y.) 171*, 308-311.
NOTON, D. and STARK, L. 1971b. Scanpaths in saccadic eye movements while viewing and recognizing patterns. *Vision Research 11*, 929-932.
RIGAS, I., ABDULIN, E. and KOMOGORTSEV, O. 2015. Towards a multi-source fusion approach for eye movement-driven recognition. *Infomation Fusion Available online: 20 August 2015*.
RIGAS, I., ECONOMOU, G. and FOTOPOULOS, S. 2012a. Biometric identification based on the eye movements and graph matching techniques. *Pattern Recognition Letters 33*, 786-792.
RIGAS, I., ECONOMOU, G. and FOTOPOULOS, S. 2012b. Human eye movements as a trait for biometrical identification. In *IEEE Fifth International Conference on Biometrics: Theory, Applications and Systems (BTAS)*, 217-222.
RIGAS, I. and KOMOGORTSEV, O.V. 2014. Biometric Recognition via Probabilistic Spatial Projection of Eye Movement Trajectories in Dynamic Visual Environments. *IEEE Transactions on Information Forensics and Security 9*, 1743-1754.
ROBINSON, D.A. 1964. The mechanics of human saccadic eye movement. *The Journal of Physiology 174*, 245-264.
SALVUCCI, D.D. and GOLDBERG, J.H. 2000. Identifying fixations and saccades in eye-tracking protocols. In *Proceedings of the 2000 Symposium on Eye Tracking Research & Applications (ETRA)*2000 ACM, 71-78.
SCHNITZER, B.S. and KOWLER, E. 2006. Eye movements during multiple readings of the same text. *Vision Research 46*, 1611-1632.
SCHUTZ, A.C., BRAUN, D.I. and GEGENFURTNER, K.R. 2011. Eye movements and perception: a selective review. *J Vis. 11*, pii: 9.
SHADMEHR, R., ORBAN DE XIVRY, J.J., XU-WILSON, M. and SHIH, T.-Y. 2010. Temporal Discounting of Reward and the Cost of Time in Motor Control. *The Journal of Neuroscience 30*, 10507-10516.
SMI 2015. RED250-RED500, http://www.smivision.com/en/gaze-and-eye-tracking-systems/products/red-red250-red-500.html.
SNELICK, R., ULUDAG, U., MINK, A., INDOVINA, M. and JAIN, A. 2005. Large-scale evaluation of multimodal biometric authentication using state-of-the-art systems. *IEEE Transactions on Pattern Analysis and Machine Intelligence (PAMI) 27*, 450-455.
THEEYETRIBE 2015. Eye Tribe Tracker, https://theeyetribe.com/.
THOMAS, J.G. 1969. The dynamics of small saccadic eye movements. *J Physiol. 200*, 109-127.
TOBII 2015. Glasses 2, http://www.tobii.com/en/eye-tracking-research/global/landingpages/tobii-glasses-2/.
VAN BEERS, R.J. 2007. The Sources of Variability in Saccadic Eye Movements. *The Journal of Neuroscience 27*, 8757-8770.
YARBUS, A.L. 1967. *Eye Movements and Vision*. Plenum Press, New York.
YINGYING, J., YONG, P., BAO-LIANG, L., XIAOPING, C., SHANGUANG, C. and CHUNHUI, W. 2014. Recognizing slow eye movement for driver fatigue detection with machine learning approach. In *2014 International Joint Conference on Neural Networks (IJCNN)*, 4035-4041.
YOON, H.-J., CARMICHAEL, T.R. and TOURASSI, G. 2014. Gaze as a biometric. In *SPIE*, 903707-903707-903707.
ZHANG, Y. and JUHOLA, M. 2012. On Biometric Verification of a User by Means of Eye Movement Data Mining. In *Second International Conference on Advances in Information Mining and Management (IMMM 2012)*, 85-90.
ZUBER, B.L., STARK, L. and COOK, G. 1965. Microsaccades and the velocity-amplitude relationship for saccadic eye movements. *Science 150*, 1459-1460.